Nayaka et al. Beni-Suef University Journal of Basic and Applied Sciences (2020) 9:51
https://doi.org/10.1186/s43088-020-00074-8

Beni-Suef University Journal of Basic and Applied Sciences

RESEARCH Open Access

Biosynthesis, characterization, and in vitro assessment on cytotoxicity of actinomycete-synthesized silver nanoparticles on *Allium cepa* root tip cells

Sreenivasa Nayaka*, Bidhayak Chakraborty, Meghashyama Prabhakara Bhat, Shashiraj Kareyallappa Nagaraja, Dattatraya Airodagi, Pallavi Sathyanarayana Swamy, Muthuraj Rudrappa, Halaswamy Hiremath, Dhanyakumara Shivapoojar Basavarajappa and Bharati Kanakannanavar

Abstract

Background: The industrial production of silver nanoparticles (AgNPs) and its commercial applications are being considerably increased in recent times, resulting in the release of AgNPs in the environment and enhanced probability of contaminations and their adverse effects on living systems. Based on this, the present study was conducted to evaluate the in vitro cytotoxicity of actinomycete-synthesized AgNPs on *Allium cepa* (*A. cepa*) root tip cells. A green synthesis method was employed for biosynthesis of AgNPs from *Streptomyces* sp. NS-33. However, morphological, physiological, biochemical, and molecular analysis were carried out to characterize the strain NS-33. Later, the synthesized AgNPs were characterized and antibacterial activity was also carried out against pathogenic bacteria. Finally, cytotoxic activity was evaluated on *A. cepa* root tip cells.

Results: Results showed the synthesis of spherical and polydispersed AgNPs with a characteristic UV-visible (UV-Vis.) spectral peak at 397 nm and average size was 32.40 nm. Energy dispersive spectroscopy (EDS) depicted the presence of silver, whereas Fourier transform infrared (FTIR) studies indicated the presence of various functional groups. The phylogenetic relatedness of *Streptomyces* sp. NS-33 was found with *Streptomyces luteosporeus* through gene sequencing. A good antibacterial potential of AgNPs was observed against two pathogenic bacteria. Concerning cytotoxicity, a gradually decreased mitotic index (MI) and increased chromosomal aberrations were observed along with the successive increase of AgNPs concentration.

Conclusions: Therefore, the release of AgNPs into the environment must be prevented, so that it cannot harm plants and other beneficial microorganisms.

Keywords: *Streptomyces luteosporeus*, Green synthesis, AgNPs, Antibacterial, Cytotoxicity

1 Background

The synthesis of different metal nanoparticles is one of the most effective areas of research in modern science. These nanoparticles show completely different properties depending on specific characteristics, such as shapes, sizes, and distributions and can be used as biological markers because of the large surface to volume ratio [1–3]. The metal nanoparticles are composed of about 20 to 15,000 atoms, which results in a size smaller than 1 to 100 nm [4, 5]. Biological and chemical properties of nanoparticles with respect to size and shape have a strong affinity to various target molecules particularly proteins, structural sturdiness in spite of atomic

* Correspondence: sreenivasanayaka06@gmail.com
P.G. Dept. of Studies in Botany, Karnatak University, Dharwad, Karnataka 580003, India

granularity, enhanced or delayed particles aggregation depending on the type of the surface modification, enhanced photoemission, high electrical and heat conductivity, and improved surface catalytic activity [2, 6]. In modern material science; nanoparticles or nanocrystals have found enormous applications in the field of therapeutics, antimicrobials, high-sensitivity bimolecular detection, diagnostics, catalysis, and microelectronics [7].

It is well known that the size and shape of nanoparticles have a great effect on their electronic and optical properties; thus, there has always been obvious interest in controlling the size, shape, and surrounding media of nanoparticles. There are different chemical, physical, and biological methods for the synthesis of nanoparticles [1, 7, 8]. The physical methods of synthesis produce large quantities of nanoparticles with definite shape and size. However, the production of large quantities of waste materials, uses of high amount of energy, time required for synthesis, and acquiring thermal stability of nanoparticles are the disadvantages of this process [1, 8, 9]. Chemical methods of synthesizing are complicated and have many effects, such as producing numerous dangerous chemicals, which are toxic in nature and produce wastes. These chemicals are harmful, not only to the environment, but also to human health [10]. The use of environmentally benign substances, like extracts of different plant parts and microorganisms do not use toxic chemicals for the synthesis of nanoparticles [7, 11, 12]. This kind of green synthesis of nanoparticles offers numerous benefits, eco-friendliness, and compatibility for pharmaceutical and other biomedical applications. This biogenic synthesis of metal nanoparticles has long been recognized having an inhibitory effect on microbes present in medical and industrial processes [4, 13]. There are many microorganisms, such as bacteria, actinomycetes, fungi, and viruses that have been investigated to produce different metal nanoparticles of silver (Ag), gold, zinc, palladium, magnesium, copper, iron, lead, titanium, etc. [11, 14, 15].

Actinomycetes are prokaryotic, gram positive bacteria with high guanine (G) and cytosine (C) contents in their deoxyribonucleic acid (DNA). These actinomycetes produce rod-shaped or coccoid cells or aerial and substrate mycelia, which resemble fungal morphology [16]. These gram-positive bacteria are phylogenetically divided into two major divisions, "low-GC" and "high-GC". Although the gram-positive bacteria with high-GC content have less adenine (A) and thymine (T) base pairs in DNA. These actinomycetes have diverse biological activities due to their capacity of production of a wide range of secondary metabolites. They are one of the largest prokaryotic groups of microbial resources having high commercial value, which contributed in production of almost half (47.01%) of the total antibiotics discovered [17, 18]. Actinomycetes are also the producer of numerous non-antibiotic bioactive metabolites, such as antioxidation reagents, immunological regulators, enzymes, enzyme inhibitors, neuritogenic, anti-cancer, anti-inflammatory, anti-helmintic, herbicides, vitamins, and pesticides [17, 19, 20]. The biosynthesis of nanoparticles occur in microorganisms, when they grab target metal ions from their environment and turn the ions into the element metal through enzymes produced by the cell activities. In particular, the biogenic synthesis of metal nanoparticles from actinomycetes may take place intracellularly or extracellularly. In actinomycetes, the intracellular reduction of metal ions takes place on the surface of mycelia along with cytoplasmic membrane or by transporting metal ions into the microbial cell in the presence of enzymes, which eventually leads to the formation of nanoparticles. The extracellular synthesis, however, involves reducing the metal ions in presence of reductase enzyme [11, 21–23].

In context to mutagenesis and cytotoxicity analysis, plants have been used as an indicator organism. The plant systems have a variety of genetic endpoints, such as alterations in ploidy, chromosomal aberrations, and sister chromatid exchanges. The plant *Allium cepa* was regarded as a bio-indicator plant for environmental pollution since 1920. The chromosomal aberrations in *A. cepa* root are an established plant bioassay and were validated by the International Programme on Chemical Safety (IPCS), World Health Organization (WHO), and the United Nations Environment Programme (UNEP). It is an efficient and standard model of biological system for the cytotoxicity of AgNPs on root meristems, chemical screening, and in situ monitoring for genotoxicity of environmental substances [24–26]. There are also some reports on the genotoxic effects of AgNPs in *Tradescantia paludosa*, *Vicia faba*, *Hordeum vulgare*, *Crepis capillaries, Pisum sativum*, *Allium sativum*, *Drimia indica*, etc. [27, 28]. Researchers have revealed that the *A. cepa* system is considered to be the best-established system, which is correlated considerably with the studies performed in eukaryotic and prokaryotic systems for evaluation of genotoxicity in vitro and in vivo [29]. In the present study the genotoxicity of soil actinomycete-synthesized AgNPs was evaluated for the first time.

2 Methods

In the present work, the actinomycetes were isolated from soil samples collected from agricultural fields, characterized, and used for the synthesis of AgNPs. Further, the synthesized AgNPs were characterized and used for *A. cepa* root tip cell bioassay for observing cytotoxicity.

2.1 Isolation and antimicrobial activities of actinomycetes

Fifteen soil samples were collected at a depth of 10 to 25 cm from agricultural fields. The collected soil samples were immediately packed in sterile plastic bags and transferred to the microbiology laboratory for analysis. At first, the samples were air-dried at room temperature (~ 25 °C) for 7 to 8 days. Later, 1 g of each soil sample was dissolved in 10 ml of autoclaved 9 g/l sodium chloride (NaCl, physiological saline), and serially diluted in down to 10^{-7}. One hundred microliters of each serially diluted sample was dispensed on starch casein agar (SCA) medium (starch, 10 g; casein, 0.30 g; potassium nitrate, 2.0 g; NaCl, 2.0 g; di-potassium hydrogen phosphate, 2.0 g; magnesium sulfate heptahydrate, heptahydrate, 0.05 g; calcium carbonate, 0.02 g; ferrous sulfate heptahydrate, 0.01 g; agar, 18.0 g; distilled water, 1 l; pH 7.0 ± 0.2), International Streptomyces Project (ISP) 2 medium (yeast extract, 4.0 g; malt extract, 10.0 g; dextrose, 4.0 g; agar, 20.0 g; distilled water, 1 l; pH 7.3 ± 0.2) and ISP6 medium (peptone, 15 g; yeast extract, 1 g; ferric ammonium citrate, 0.500 g; sodium thiosulfate, 0.080 g; di-potassium hydrogen phosphate, 1.0 g; agar, 15 g; distilled water, 1 l; pH 7.0 ± 0.2) supplemented with nystatin and cycloheximide (50 μg/ml), respectively. The plates were incubated at 33 °C for 7 to 8 days for isolation of actinomycetes. All the isolated actinomycetes strains were used to perform antimicrobial screening by cross streak method. Each strain was grown as a single streak on nutrient agar medium and incubated at 33 °C for 7 to 8 days. The pathogenic organisms were streaked at the angle of 90° to actinomycetes streak and incubated at 37 °C for 24 h [30–32]. After incubation, the most active strain designated as *Streptomyces* sp. NS-33, which inhibited the growth of pathogens was used for the synthesis of AgNPs.

2.2 Characterization of *Streptomyces* sp. NS-33

2.2.1 Morphological, physiological, and biochemical characterization

For morphological characterizations, the *Streptomyces* sp. NS-33 was grown for 7 to 9 days on SCA, ISP2, ISP3, ISP4, ISP5, and ISP6 media. The pH of all media was adjusted at pH 7.0. The shape of the colony, pigmentation and color of aerial, and substrate mycelia was observed in each medium and recorded. The spore surface morphology of *Streptomyces* sp. NS-33 was observed under a scanning electron microscope (SEM) (JSM-IT500, In Touch Scope Scanning Electron Microscope) by cover-slip culture method at a resolution of × 10,000 [33]. Physiological characterization was done to check the growth of the organism at different temperatures ranging from 20 to 60 °C, pH tolerance from pH 4.0 to 9.0 and NaCl tolerance at different concentrations up to 7%. In order to record the biochemical characteristics, the *Streptomyces* sp. NS-33 was used for the hydrolysis of urea and gelatin. Hydrogen sulfide (H_2S), indole production, citrate utilization, gram staining, and motility were also checked. Further, analysis of the utilization of carbon sources was done on D-glucose, sucrose, mannitol, inositol, rhamnose, sorbitol, trehalose, and xylose [34].

2.2.2 Molecular characterization

The molecular taxonomical identification of the *Streptomyces* sp. NS-33 was done by 16S ribosomal Ribonucleic Acid (16S rRNA) gene sequencing. Genomic DNA was extracted and purified using Hi-PurA *Streptomyces* DNA Purification Kit (MB527) according to the manufacturers' protocol. Briefly, the *Streptomyces* sp. NS-33 culture was centrifuged (Remi R-8C) at 10,000 rpm to remove the culture medium. The obtained pellet was re-suspended in 300 μl lysis solution and 20 μl of RNase A solution and incubated at 25 °C for 2 min. Twenty microliters of protinase-K solution was added and incubated at 55 °C for 30 min. This mixture was later vortexed horizontally at the maximum speed for 7 min and incubated at 95 °C for 10 min. The mixture was centrifuged at 12,000 rpm for 1 min and 200 μl of lysis solution was added, vortexed for 15 s and incubated at 55 °C for 10 min. To this homogenous mixture 200 μl of ethanol was added and vortexed for 15 s. The lysate was then transferred to a Hi-Elute Miniprep Spin column and 500 μl of prewash solution was added and centrifuged at 10,000 rpm for 1 min and the supernatant was discarded. To this pellet, 500 μl of wash solution was added and centrifuged for 3 min at 12,000 rpm; the supernatant was discarded. Two hundred microliters of elution buffer was pipetted into the column and incubated for 1 min at room temperature. The DNA was eluted finally by centrifugation at 10,000 rpm for 1 min. The region of 16S rRNA was amplified through polymerase chain reaction (PCR) using forward primer (5′-GGTTACCTTG TTACGACTT-3′) and reverse primer (5′-AGAGTTTG ATCCTGGCTCAG-3′). PCR reaction was carried out in final volume of 50 μl. The reaction mixture contained template DNA 1.0 μl, buffer 5 μl (free from Mg^{2+}), magnesium chloride 5 μl (2.5 μM), deoxyribonucleotide triphosphates (dntps) 8 μl (2.5 μM each dATP, dTTP, dGTP, dCTP), primer 1 μl each (20 μM each), *Taq* DNA polymerase 0.5 μl (5.0 U/μl), and molecular grade water to make up the volume up to 50 μl. The whole reaction mixture was amplified in an Applied Biosystems 2720 Thermal Cycler. The PCR cycles were programmed as follows, initialization for 5 min at 96 °C, denaturation for 30 s at 96 °C, followed by annealing at 55 °C for 30 s, extension for 90 s at 72 °C and final extension at 72 °C for 10 min [30]. Later, PCR products were electrophoresed on 1% agarose gel with a 500-bp DNA ladder for size

reference. The purified PCR amplicon was sequenced, compiled and matched with the Gene Bank database using Basic Local Alignment Search Tool (BLAST) on the National Center for Biotechnology Information (NCBI) website. Further, the DNA sequence was aligned with the aid of CLUSTAL-X software and a phylogenetic tree was constructed by the neighbor-joining method using MEGA 7.0 software [32, 35, 36].

2.3 Biosynthesis of AgNPs

The *Streptomyces* sp. NS-33 was grown in starch casein broth with continuous shaking on a rotary shaker (120 rpm) at 33 °C for 7 to 9 days. Later, the broth was centrifuged at 8000 rpm for 20 min to separate the biomass. For the synthesis of AgNPs, an equal volume of cell-free supernatant and aqueous silver nitrate ($AgNO_3$) (1mMol/l) solution was interacted at a pH adjustment 8.0. The interacted solution was kept in the dark on a rotary shaker (120 rpm) at 28 °C for 4 days. Pure double-distilled water was used in control experiments [37].

2.4 Characterizations of AgNPs

The probable formation of AgNPs in aqueous solution was observed by the change of color of the solution. Later, a physicochemical analysis was performed by measuring UV-visible (UV-Vis.) spectrum at 350 to 700 nm to confirm the formation of AgNPs using a UV-Vis. spectrophotometer (UV-9600A, Metash Instruments Co. Ltd., Shanghai, China) [38]. The size, shape, and surface morphology of AgNPs were analyzed using atomic force microscopy (AFM). The sample for AFM was prepared by making a suspension of AgNPs with water and the addition of a droplet onto a substrate. The air-dried suspension was scanned using an AFM instrument (FLEX-AFM, Nanosurf easyscan II controller) [39]. In order to identify the biological functional groups the dried *Streptomyces* sp. NS-33 supernatant and AgNPs were mixed with potassium bromide and thin disks were made, which was scanned in the range of 400 to 4000 cm^{-1} at prominent infrared resonance spectra by Fourier transform infrared (FTIR) spectrophotometer (Nicolet 6700, Thermo Fisher Scientific, Waltham, Massachusetts, USA) [40]. Moreover, the size and shape of AgNPs were also observed by transmission electron microscope (TEM) analysis. For this, AgNPs were diluted with sterile double-distilled water and applied onto a carbon-coated copper grid and allowed to dry at room temperature for 15 min under infrared light. This was further photographed using TEM (FEI, TECNAI G2, F30) at a magnification of × 60,000 to × 80,000 [41]. Elemental analysis was done using Energy dispersive spectroscopy (EDS) coupled with SEM to identify the metal ion concentration in AgNPs [39]. Finally, X-ray diffraction (XRD) measurements of AgNPs were performed using XRD spectroscopy (Rigaku Smartlab SE). The sample was prepared placing AgNPs powder into a sample holder and a smooth surface was made through pressing. The XRD spectra were recorded between 30 and 80° by X-ray diffractometer equipped with CuKα filter (λ = 0.15418 nm), 2θ/θ scanning mode. The obtained diffractogram was compared to the standard Joint Committee on Powder Diffraction Standards (JCPDS) card no. 04-0783. At last, the size of AgNPs was estimated using Debye Scherrer's formula, $d = k\lambda/\beta\cos\theta$, where, k = Debye Scherrer's constant 0.89, λ = the wavelength (0.15418 nm), β = FWHM of Bragg's peaks, and θ = value of Bragg's angle [46].

2.5 Antibacterial activity of AgNPs

The antibacterial activity of AgNPs was tested against human pathogenic bacteria through a well diffusion assay. Three gram-positive bacteria, such as *Staphylococcus aureus* (MTCC6908), *Streptococcus pneumoniae* (MTCC2672), *Enterococcus faecalis* (MTCC6845), and a gram-negative bacterium *Escherichia coli* (MTCC40) were collected from MTCC, Pune. One hundred micro liters of each fresh culture of pathogenic bacteria was spread on the plates containing Mueller-Hinton agar medium. One milligram AgNPs was diluted with 1 ml of double-distilled water and vortexed thoroughly to make a proper suspension. Further, 6-mm wells were made and different volumes of AgNPs, such as 25 μl, 50 μl, 75 μl, and 100 μl, were loaded into each well. One hundred microliters of $AgNO_3$ and 100 μl of *Streptomyces* sp. NS-33 supernatant were also loaded to compare results with AgNPs suspension. Later, the plates were incubated at 37 °C for 24 h and the zone of inhibition was measured in millimeters [7].

2.6 Assessment of cytotoxic activity on *Allium cepa* root tip cells

Healthy onion bulbs were bought from the local market and used for growing roots. Briefly, the outer dry scale leaves and dry roots were removed from bulbs without damaging the root primordia. The bulbs were then kept in coupling jars containing distilled water for growing roots in laboratory temperature (approximately 26 °C) for 4 to 5 days. The distilled water in coupling jars was changed every day. Later, the onions with newly grown roots were treated with 25 μg/ml, 50 μg/ml, 75 μg/ml, and 100 μg/ml AgNPs suspension for 24 h. The control experiment was done by keeping the onions in sterile distilled water. Both the experiments were carried out in laboratory temperature (approximately 26 °C). After 24 h of treatment the roots were cut in 5 mm length and fixed in Carnoy's solution [ethyl alcohol to glacial acetic acid (3:1)] for 24 h and then preserved in 70% alcohol at 4 °C. A squash was prepared by taking the meristematic region of roots and using 2% acetocarmine dye. The

slides were observed under a microscope (Olympus CX23, Binocular microscope) for counting the cells under division and various chromosomal aberrations in each concentration or treatment. The observation of cells under microscope was done in quadruplicate for each concentration of AgNPs and around 1500 cells were counted. The mitotic index (MI) was calculated using the following formula [26, 28].

$$\text{MI}\ (\%)\ \frac{\text{Number of cells in mitosis}}{\text{Total number of cells}} \times 100$$

2.7 Statistical analysis

The Statistical Package for the Social Sciences-20 (SPSS-20) software was used for statistical analysis followed by one way analysis of variance (ANOVA) and standard deviation (± SD) in representation of data.

3 Results

3.1 Isolation of actinomycetes

During the screening 37 actinomycetes strains were isolated from different agricultural field soil samples. Interestingly, out of 37 isolated actinomycetes strains, the *Streptomyces* sp. NS-33 showed significant antimicrobial activity through cross streak method and was selected as a potential strain for studies.

3.2 Characterizations of *Streptomyces* sp. NS-33

3.2.1 Morphological, physiological, and biochemical characterizations

The observations of morphological, physiological, and biochemical characterizations were listed in Table 1. The *Streptomyces* sp. NS-33 showed a range of color of aerial and substrate mycelium on SCA, ISP2 to ISP6 media. However, the organism did not produce any pigment on ISP media, but a light yellow pigmentation was found on SCA medium (Fig. 1). The colony formed by the strain NS-33 was irregular in shape with a flat surface. The spore chain morphology of *Streptomyces* sp. NS-33 showed ovoid to doliform spores having a smooth surface with slight depression at three sides. The spore chain was poly-sporus in which the spores were attached in an end to end fashion forming retinaculiapreti structure (Fig. 2). During physiological characterizations, optimum growth of the strain NS-33 was found at 33 to 35 °C, whereas a weak and no growth was noted below and above this temperature range. The strain NS-33 was found to grow best at pH 7.0 and 3 to 4% NaCl concentration, but a relatively weak growth was noted at pH 8.0. At last, the biochemical characterizations revealed that the isolate was gram-positive with non-motile spores. The strain NS-33 showed positive results only for hydrolysis of gelatin and urea, while a negative result was obtained for indole, H_2S production, and citrate utilization. The most utilized carbon sources by the strain NS-33 were D-glucose, inositol, and trehalose, while there was no growth observed on sucrose, mannitol, inositol, raffinose, sorbitol, and xylose (Table 1).

3.2.2 Molecular characterization

The molecular characterization of the *Streptomyces* sp. NS-33 was achieved by 16S rRNA sequencing. The genomic DNA was extracted and the region of 16S rRNA was amplified using primers. The obtained 16S rRNA partial sequencing was linear and 742 bp in length, which was deposited to the NCBI database of gene bank with accession number MN587998. This was further subjected to BLAST analysis in search of close relatedness with other *Streptomyces* spp. The BLAST result showed 98.18% sequence similarity with *Streptomyces luteosporeus* strain NBRC-14657 (NR112439). Further, a phylogenetic tree analysis of *Streptomyces* sp. NS-33 revealed its evolutionary relationship with *Streptomyces luteosporeus* strain NBRC-14657 (NR112439) as shown in Fig. 3.

3.3 Biosynthesis of AgNPs

During the synthesis, the color of *Streptomyces* sp. NS-33 cell-free supernatant was changed from pale-yellow to brown color after mixing and incubation with an equal volume of $AgNO_3$ at pH 8.0. This indicated the formation of AgNPs (Fig. 4).

3.4 Characterizations of AgNPs

3.4.1 UV-Vis. spectroscopy

The UV-Vis. spectroscopic analysis of AgNPs was carried out after 4 days of incubation in dark condition. The color of the reaction mixture was changed from pale-yellow to brown. The characteristic absorption peak of synthesized AgNPs was obtained at 397 nm, which confirmed their formation (Fig. 5).

3.4.2 AFM analysis

The two and three dimensional AFM topography images of AgNPs were used to study the size, shape, and surface morphology. The images revealed that the AgNPs were well defined, spherical in shape, and were polydispersed in nature with a size ranged between 25 and 78 nm. The size distribution of the AgNPs was shown in Fig. 6. The data obtained from AFM analysis was correlated with TEM results.

3.4.3 FTIR analysis

The FTIR spectra of *Streptomyces* sp. NS-33 supernatant and biosynthesized AgNPs were depicted in Fig. 7a and b, respectively. Several vibrational frequencies were observed in the range of 400 to 4000 cm^{-1}. The FTIR

Table 1 Biochemical characterizations of *Streptomyces* sp. NS-33

Morphological characterizations			
Medium	**Color of aerial mycelium**	**Color of substrate mycelium**	**Pigmentation**
SCA	White	Light yellow	Light yellow
ISP-2	White	Yellow	-
ISP-3	Grayish	Light brown	-
ISP-4	Pinkish	Light brown	-
ISP-5	White	Light yellow	-
ISP-6	Beige	Light yellow	-
Colony morphology of *Streptomyces* NS-33		Irregular margin with a flat surface	
Physiological characterizations			
Growth at different temperatures			
20 °C		-	
25 °C		W	
30 °C		++	
35 °C		++	
40 °C		W	
45 °C		-	
50 °C		-	
55 °C		-	
60 °C		-	
Growth at different pH and NaCl concentration			
pH 4		-	
pH 5		-	
pH 6		-	
pH 7		++	
pH 8		W	
pH 9		-	
NaCl concentration		3 to 4%	
Biochemical characterizations			
Gram staining		Gram-positive	
Motility		Non-motile	
Indole		-	
Citrate utilization		-	
H_2S production		-	
Urea		+	
Gelatin		+	
D-glucose		+	
Sucrose		-	
Mannitol		-	
Inositol		+	
Raffinose		-	
Sorbitol		-	
Trehalose		+	
Xylose		-	

- Negative, *W* Weak, + Positive, ++ Good growth

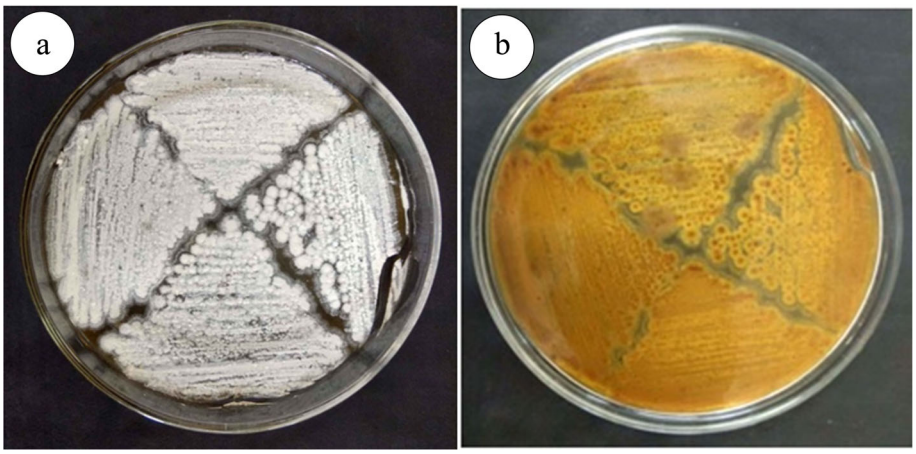

Fig. 1 Growth of *Streptomyces* sp. NS-33 on SCA medium. **a** Aerial mycelium (white). **b** Substrate mycelium (light yellow pigmentation)

spectrum of NS-33 supernatant revealed eleven absorption peaks, positioned at 3400, 2953, 2372, 2355, 1659, 1310, 1142, 1088, 1016, 927, and 656 cm^{-1}, whereas the AgNPs illustrated peaks at following wave numbers 3440, 2941, 2364, 2357, 1664, 1385, 1132, 1065, 1020, 929, and 669 cm^{-1}. The first strong and broad absorption peak at 3400–3440 cm^{-1} arose due to the presence of an O-H stretching vibration of alcohol. The peak shifting from 2953 to 2941 cm^{-1} was attributed to C-H medium stretching of alkane, while the spectral peak at 2372 to 2364 cm^{-1} indicated a vibration of P-H phosphine. The weak vibrational peaks positioned at 2355 to 2357 cm^{-1} were also attributed to P-H vibration of phosphine. However, the intense peak at 1659–1664 cm^{-1} was assigned to C=C stretching of alkene and the peak 1310–1385 cm^{-1} was indicated an O-H bending vibration of phenol. In addition to these, the weak peak at 1142–1132 cm^{-1} was attributed to C-N stretching of a secondary amine, whereas the peak positioned at 1088–1065 cm^{-1} indicated to C-O stretching of alkyl substituted ether and the peak at 1016–1020 cm^{-1} attributed to C-F stretching of alkyl halides. Finally, the 2-weak peaks positioned at 927–929 cm^{-1} and 656–669 cm^{-1} were assigned to ring vibration of cyclohexane and C-H bending of alkyne, respectively.

3.4.4 TEM analysis

The size, morphology, and distribution of the AgNPs were characterized by TEM, which was shown in Fig. 8. The AgNPs appeared oval to spherical in shape (Fig. 8a), polydispersed, scattered, and the size ranged from 22 to 75 nm (Fig. 8b). The average size of nanoparticles was found at 30.35 nm.

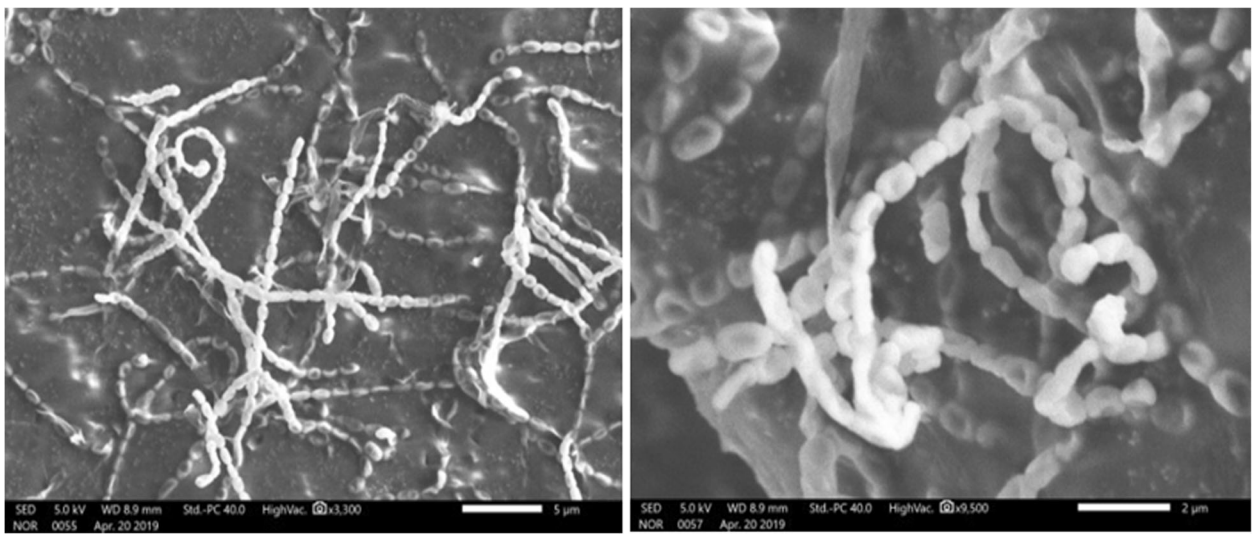

Fig. 2 SEM micrograph showing the morphology of *Streptomyces* sp. NS-33

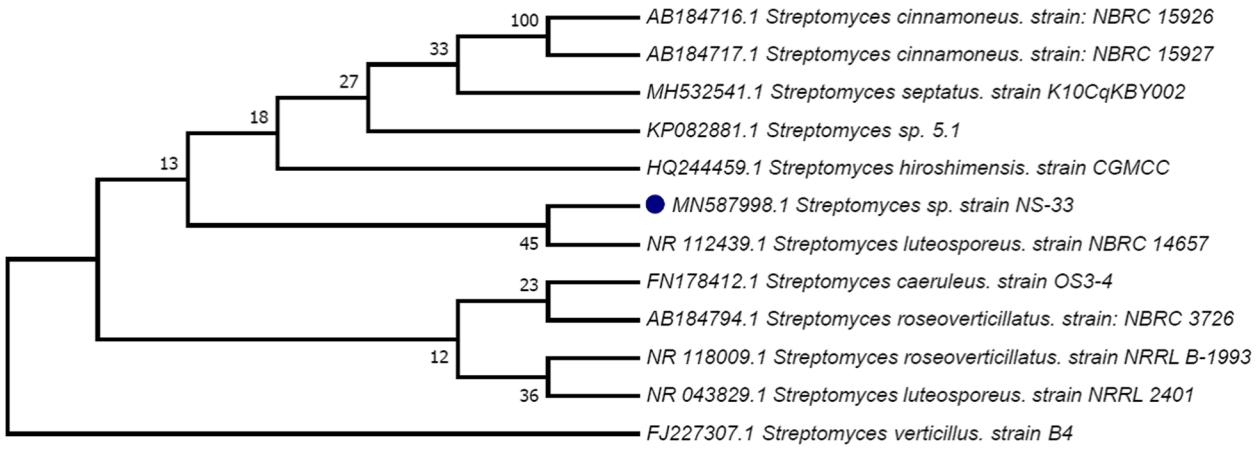

Fig. 3 Phylogenetic tree of *Streptomyces* sp. NS-33 showing the evolutionary relationship

3.4.5 EDS analysis

The EDS spectrum of AgNPs expressed qualitative and quantitative compositions of different components that may be present in the formation of AgNPs. The spectrum showed a strong signal at 3 KeV due to the presence of silver as the ingredient element (mass 29.03%). The other elements present in the formation of AgNPs were carbon, cobalt, sodium, magnesium, chlorine, and potassium, which were present in trace amounts (Fig. 9).

3.4.6 XRD analysis

The crystalline structure and size of the nanoparticles were determined using XRD analysis. Figure 10 revealed the characteristic diffraction peaks for AgNPs at 38.29°,

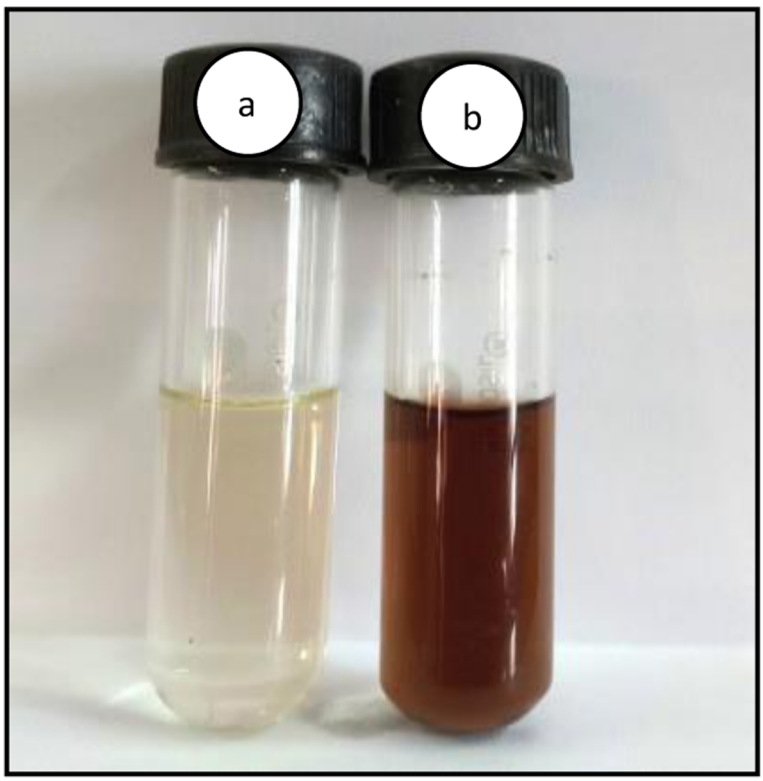

Fig. 4 Change in color of *Streptomyces* sp. NS-33 supernatant after mixing and incubation with $AgNO_3$. (a) *Streptomyces* sp. NS-33 supernatant (pale yellow). (b) The formation of AgNP suspension (brown)

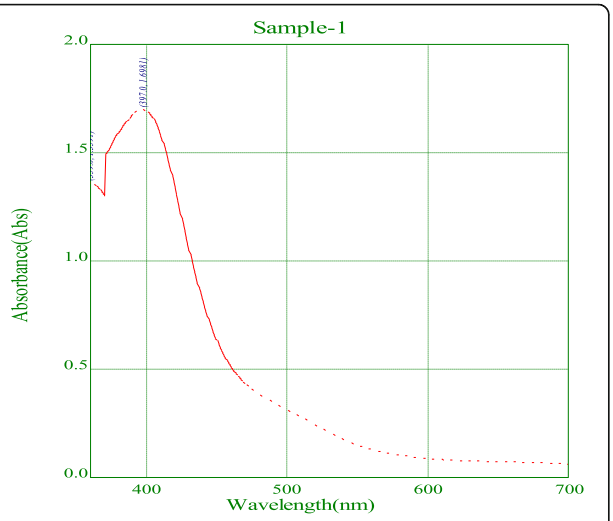

Fig. 5 UV-Vis. absorption spectrum AgNPs synthesized by *Streptomyces* sp. NS-33

46.39°, 64.62°, and 76.85°. The XRD planes obtained at (111), (200), (220), and (311) corresponded to face-centered cubic crystals of silver. The average size of the AgNPs formed in the process was calculated to be 32.40 nm.

3.5 Antibacterial activity of AgNPs

The synthesized AgNPs showed moderate antibacterial activity against different pathogenic bacteria, such as *S. aureus* (MTCC6908), *S. pneumoniae* (MTCC2672), *E. faecalis* (MTCC6845), and *E. coli* (MTCC40) (Figs. 11 and 12. Only two among the four pathogens were found susceptible to 100 μl of AgNPs suspension (Fig. 11a–d). The pathogens *S. aureus* and *S. pneumoniae* showed susceptibility to all volumes of AgNPs and even only these two pathogens showed susceptibility to 100 μl of *Streptomyces* sp. NS-33 supernatant (Fig. 11a, b). The other two organisms, such as *E. faecalis* and *E. coli,* were resistant to 25 μl to 100 μl volume of AgNPs and even to 100 μl of *Streptomyces* sp. NS-33 supernatant (Fig. 11c, d).

3.6 Cytotoxicity assay of *Streptomyces* sp. NS-33-synthesized AgNPs

The impact of different concentrations of AgNPs suspension on cell division of *A. cepa* was analyzed. The MI was highest in control, i.e., in sterile distilled water, where no chromosomal aberrations were observed. Figure 13 depicted the mitotic phases in control experiment and various chromosomal distortions after treatment with AgNPs for 24 h. A decline in the MI was noticed with the increase in the concentration of AgNPs. The lowest number of chromosomal aberrations was observed in 25 μg/ml concentration of AgNPs, which was increasing gradually with increasing concentrations of AgNPs, i.e., 50 μg/ml, 75 μg/ml, and 100 μg/ml AgNPs. In 25 μg/ml suspension of AgNPs, the MI was 60.1%. Different chromosomal aberrations including sticky chromosome, disturbed chromosome, and chromosome break were observed. In 50 μg/ml, the chromosomal aberrations observed were disturbed chromosome, laggard chromosome, multinuclear cells, etc. with a MI 50.74%. Moreover, in 75 μg/ml and 100 μg/ml of AgNPs, the MI was reduced to less than 50%, i.e., 41.35% and 28.99%, respectively, showing various chromosomal aberrations, such as chromosome break, disturbed chromosome, sticky chromosome, diagonal anaphase, and clumped metaphase (Table 2).

4 Discussions

The actinomycetes possess an important and ubiquitous group of organisms and are widely distributed in all most all natural ecosystems even at harshest ecosystems. Actinomycetes are extensively being used since the past few decades due to their capacity for the production of strong antibiotics. These microorganisms were originally called "Ray Fungi", because of their phenotypic characteristics. However, it has been strongly proved later that

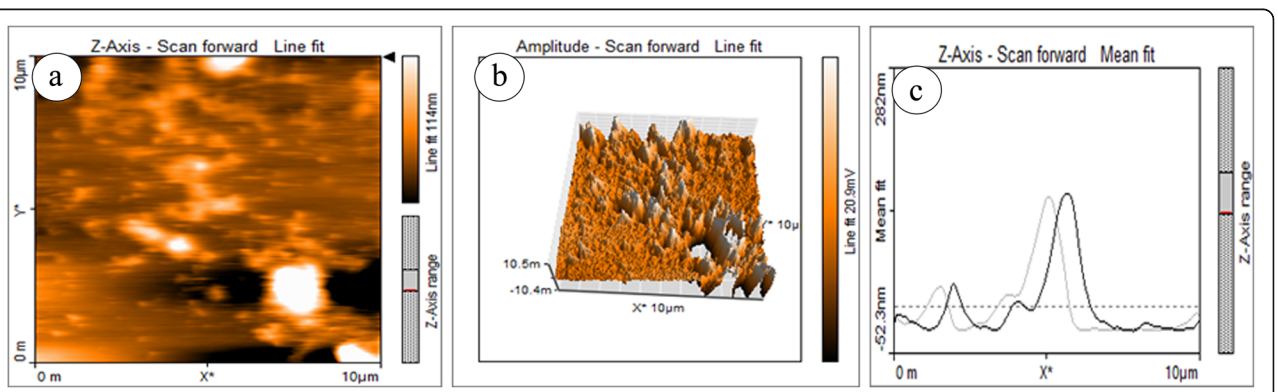

Fig. 6 Atomic force microscopy images. **a** Size of the AgNPs. **b** Height of AgNPs (3D). **c** Histogram of AgNPs

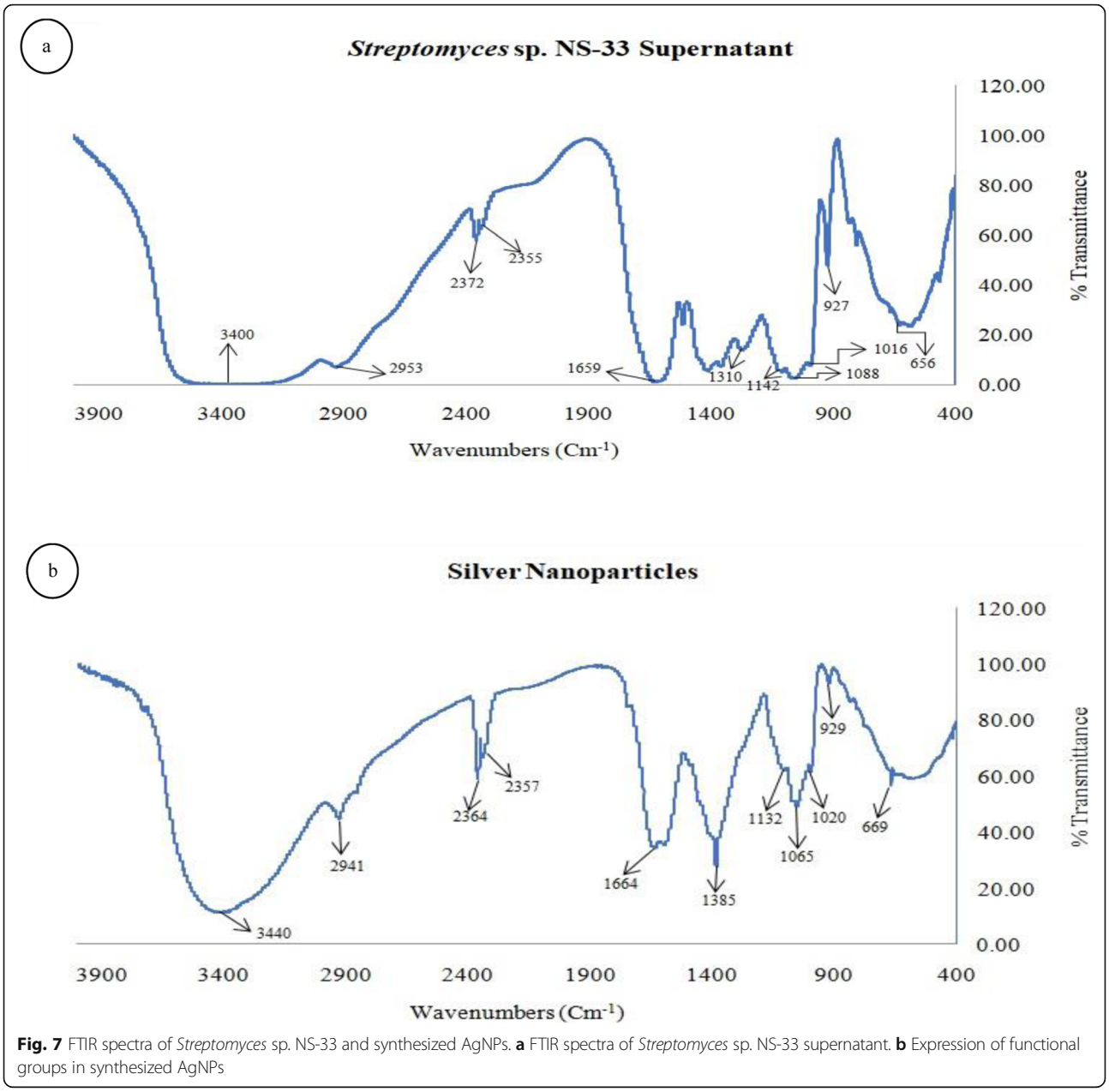

Fig. 7 FTIR spectra of *Streptomyces* sp. NS-33 and synthesized AgNPs. **a** FTIR spectra of *Streptomyces* sp. NS-33 supernatant. **b** Expression of functional groups in synthesized AgNPs

these microorganisms have a close relationship with Mycobacteria and Coryneforms and having no phylogenetic relationship with fungi [42]. In the present study, a total of 37 actinomycetes strains were isolated from soil samples collected from agricultural fields through the serial dilution method. Among these 37 isolated actinomycetes strains, the *Streptomyces* sp. NS-33 was found most active during primary screening and thereafter taken for further characterizations and synthesis of AgNPs. A similar result was demonstrated by Sreenivasa et al. [43]. Later, the *Streptomyces* sp. NS-33 was characterized through morphological, physiological, and biochemical analyses. The morphological characterizations revealed a different range of colors of aerial and substrate mycelia. The color of aerial mycelium was white to beige, while the substrate mycelium was from light yellow to light brown in color. There was a faint yellowish pigment found only on the SCA medium. This may be due to the presence of various medium compositions, which influence the color of aerial and substrate mycelium and pigmentation. The surface morphology of *Streptomyces* sp. NS-33 through SEM analysis showed smooth, ovoid to doliform spores arranged in a retinaculiapreti fashion. A similar result was reported by Priyanka et al. [33], where SEM analysis revealed the aerial mycelium of a *Nocardia* sp. PB-52 formed long,

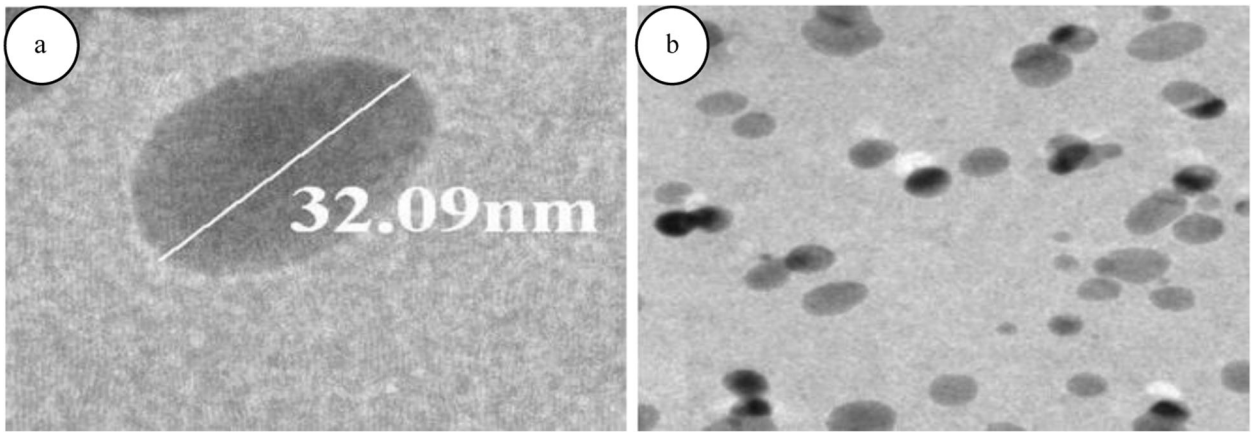

Fig. 8 TEM micrograph of *Streptomyces* sp. NS-33 synthesized AgNPs. **a** Single spherical shaped AgNP. **b** Polydispersed and scattered AgNPs

straight to rectiflexibiles spore chains having rugose spore surface. The physiological characteristics revealed the strain NS-33 was able to withstand temperatures up to 35 °C and pH 7.0. The best growth of the strain NS-33 was found only at 3 to 4% NaCl concentration. So this result showed the *Streptomyces* sp. NS-33 was a mesophilic, neutrophilic, and slightly halo-tolerant organism. The biochemical analysis indicated the capacity of strain NS-33 to hydrolyze urea, gelatin, D-glucose, inositol, and trehalose. The results obtained from morphological, physiological, and biochemical characterizations were compared with *Streptomyces* species reported in Bergey's manual of systematic bacteriology [44].

Nowadays, the 16S rRNA gene sequencing of actinomycetes has become a useful method for the identification and classification up to the species level. The 16S rRNA gene is a highly conserved region and is a component of the 30S small subunit of a prokaryotic ribosome. The sequence obtained was 742 bp long and the strain NS-33 was phylogenetically related to the *Streptomyces luteosporeus* strain NBRC-14657 (NR112439). This is because the 16S rRNA gene contains both hypervariable and conserved regions. The conserved regions are used for universal primer binding sites and hypervariable regions provide species-specific signature sequences that allow the discrimination between different specific microorganisms, such as bacteria, archaea, and microbial eukarya [45].

The nanoparticles can be synthesized from various metals, such as silver, gold, zinc, and platinum, and have a large number of biological applications. The biosynthesized AgNPs

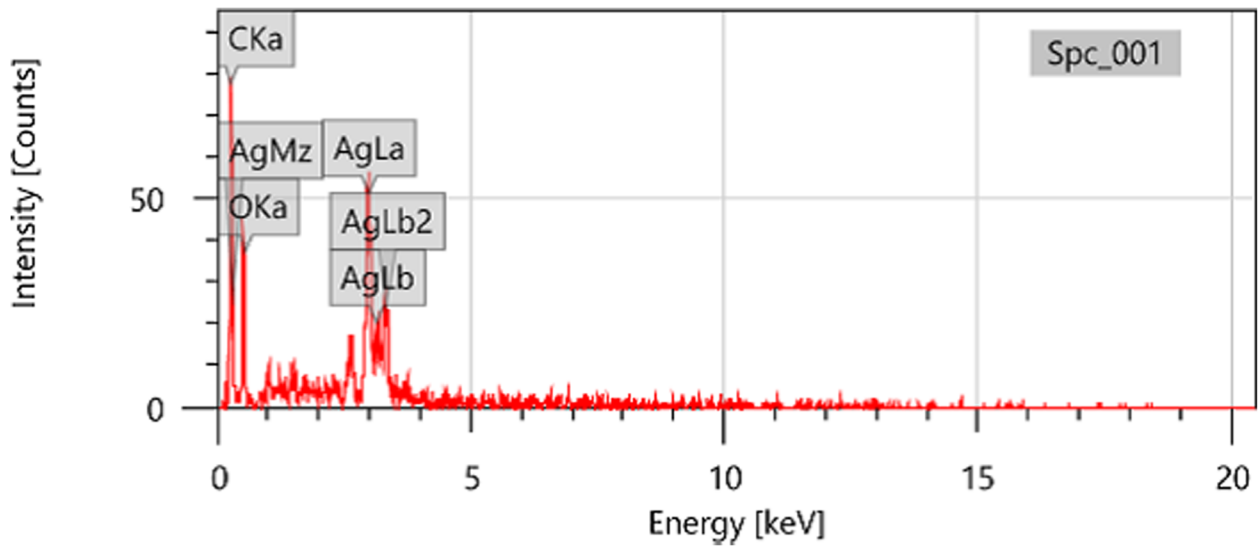

Fig. 9 EDS spectrum AgNPs synthesized by *Streptomyces* sp. NS-33

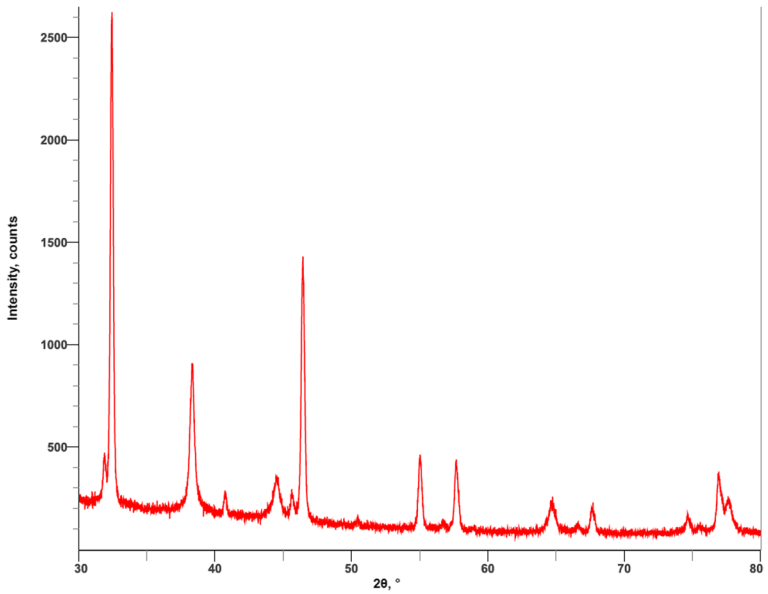

Fig. 10 XRD spectrum of biogenic AgNPs synthesized by *Streptomyces* sp. NS-33

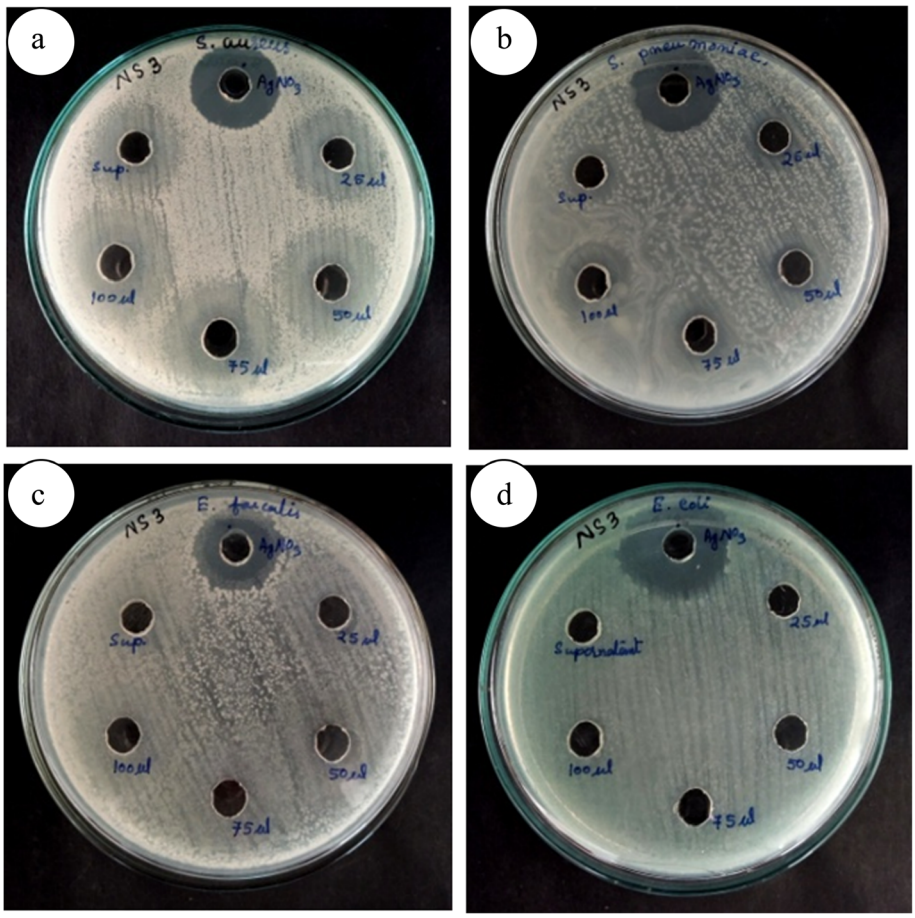

Fig. 11 Antibacterial activity of AgNPs synthesized by *Streptomyces* sp. NS-33 by well diffusion method. **a** *S. aureus*. **b** *S. pneumoniae*. **c** *E. faecalis*. **d** *E. coli*

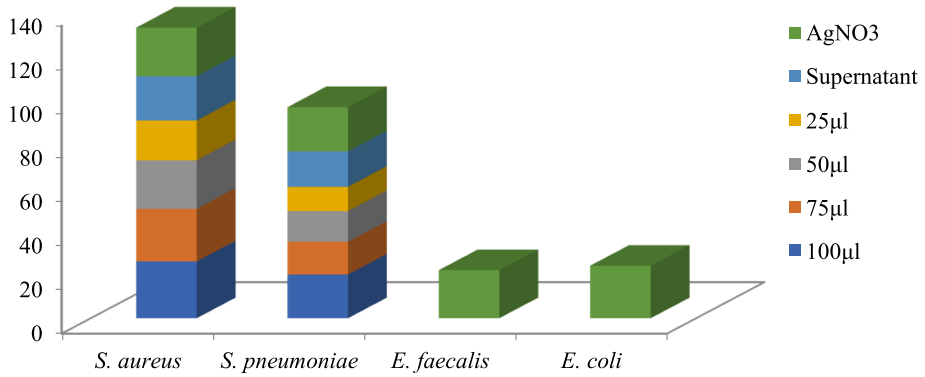

Fig. 12 Bar graph of *Streptomyces* sp. NS-33 synthesized AgNPs indicating the zone of inhibition

are comparatively less toxic to nature and have potential to suppress the growth of different pathogenic microorganisms and strong antiviral and anti-cancer properties as well. The extracellular synthesis of AgNPs from *Streptomyces* sp. NS-33 was obtained by adding 1 mMol/l $AgNO_3$ to the strain culture supernatant at pH 8.0. The change of the color from pale-yellow to brown after 4 days of incubation in the dark indicated the synthesis of AgNPs. This change of color to brown was due to the excitation of the surface plasmon in vibration with the incident light. This phenomenon is known

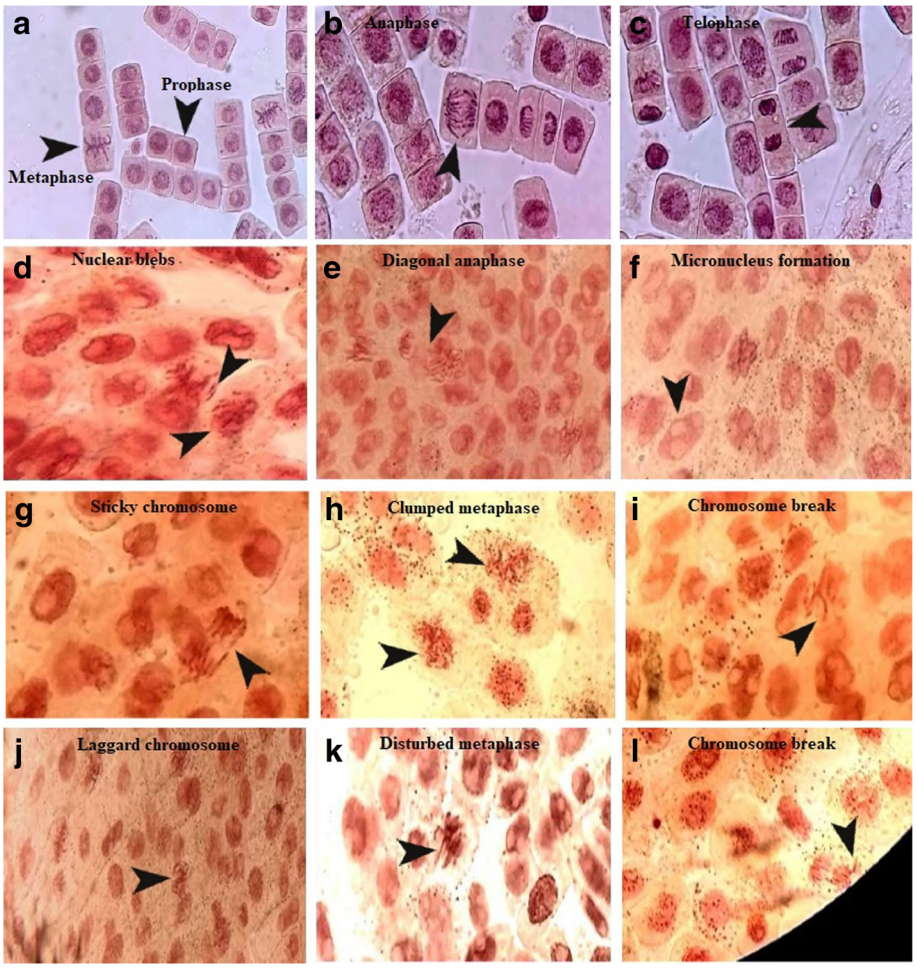

Fig. 13 Mitotic phases of *A. cepa* root tip cells in control experiment (**a**–**c**) and various aberrant features observed in the root tip cells upon exposure to AgNPs suspension (**d**–**l**)

Table 2 Distribution of *A. cepa* root tip cells treated with different the concentration of AgNPs

Sl. no.	Different concentrations of AgNPs	No. of cells counted	No. of dividing cells	Prophase	Metaphase	Anaphase	Telophase	Mitotic index [%]	Mean (± SD)
1	**Control**								
	Slide-1	348	278	244	21	8	5	79.88	**65 ± 1.66%**
	Slide-2	412	210	187	14	7	2	50.97	
	Slide-3	350	284	254	11	10	9	81.14	
	Slide-4	372	180	154	15	9	2	48.38	
2	**25 µg/ml**								
	Slide 1	409	274	262	7	3	2	66.99	**60.1 ± 1.56%**
	Slide 2	397	196	174	10	5	7	49.37	
	Slide 3	378	170	154	9	4	3	44.97	
	Slide 4	325	257	250	1	4	2	79.07	
3	**50 µg/ml**								
	Slide 1	355	178	167	5	5	1	50.14	**50.74 ± 0.49%**
	Slide 2	382	205	193	7	4	1	53.66	
	Slide 3	390	195	184	8	3	0	50	
	Slide 4	370	182	166	9	5	2	49.18	
4	**75 µg/ml**								
	Slide 1	405	162	161	1	0	0	40	**41.35 ± 1.63%**
	Slide 2	368	134	130	3	0	1	36.41	
	Slide 3	389	137	131	1	3	2	35.21	
	Slide 4	340	183	179	1	2	1	53.82	
5	**100 µg/ml**								
	Slide 1	368	111	109	1	1	0	30.16	**28.99 ± 0.99**%
	Slide 2	391	106	105	1	0	0	27.10	
	Slide 3	409	122	122	0	0	0	29.82	
	Slide 4	339	98	97	0	1	0	28.90	

as surface plasmon resonance (SPR), which is typical for AgNPs [46]. The absorption peak was obtained at 397 nm in UV-Vis. spectrophotometric analysis, which confirmed the presence of AgNPs. This is because of the unique optical properties of AgNPs, which has a strong interaction with specific light wavelengths [1]. Similar work was reported by Saminathan [47], where the strong characteristic absorbance peak at around 450 nm was observed in the AgNPs synthesized by soil *Streptomyces* sp. The present study was similar to the reports of Feng et al. [1] and Karthik et al. [48], who claimed that the reduction of $AgNO_3$ by actinomycetes could be due to the enhancing action of the extracellular nitrate reductase enzyme. The enzyme nitrate reductase is very important for the biological synthesis of AgNPs and involved in reduction of Ag^+ ions through an electron shuttle enzymatic metal reduction process. The synthesis of the AgNPs by a biological method was evidenced with the help of AFM, TEM, and XRD analysis. The AFM analysis indicated that the AgNPs were polydispersed in nature, well defined with the size ranging from 25 to 78 nm. This finding was supported by previous result of the AgNPs pattern by AFM analysis according to Asma et al. [49]. The EDS spectrum of AgNPs showed a strong typical peak at 3 KeV, which revealed the presence of silver as an ingredient element. The strong peak at 3 KeV is generally due to SPR of silver [48]. The observed result was in accordance with earlier report, where the formation of AgNPs was in the range 2 to 4 keV using *Streptomyces* sp.-Al-Dhabi-87 [37]. The identification of responsible functional groups and their proper involvement in synthesis, stabilization, and capping of AgNPs were inferred through FTIR spectroscopic analysis of *Streptomyces* sp. NS-33 supernatant and biosynthesized AgNPs. The comparative shifting of peaks in FTIR spectra ascertained the involvement of bio-molecules of *Streptomyces* sp. NS-33 supernatant in the formation of AgNPs. The O-H stretching of alcohol and C=C stretching of alkenes may be involved in stabilization of AgNPs. It was noted that C-N stretching of secondary amines of amino acids, peptides, and proteins cooperate with the formation of AgNPs. The protein molecules in strain NS-33 supernatant form a covering around free Ag^+ ions, which form AgNPs and thereby restrain them from agglomeration [21]. The microbial culture supernatant contains

various polysaccharides, terpenoids, flavonoids, and phenolic compounds, which are responsible for the reduction and capping of AgNPs [50]. TEM is a frequently used and important qualitative method for the characterization of nanomaterials to obtain measures of particle size, distribution, and morphology. Here, the size of AgNPs was in the range of 22 to 75 nm and oval to spherical in shape. The small and spherical sizes of nanoparticles have the ability to penetrate microbial cells and execute their bactericidal properties. This result was supported by the observations of Masum et al. [51].

The XRD pattern of the AgNPs was recorded using CuKα radiation, 40 kV–40 mA, 2θ/θ scanning mode, with the 2θ range of 30 to 80°. The peaks obtained in the diffractogram corresponded to 2θ values and were compared with the standard powder diffraction card of JCPDS, silver file no. 04-0783, which confirmed the resultant particles were AgNPs having a face-centered cubic crystal structure. There were 5 more peaks in the XRD diffractogram at 32.41°, 44.56°, 54.98°, 57.62°, and 67.60°. Presence of these peaks may be due to $AgNO_3$, which might have not been reduced and hence remained in the sample in minute quantity or may be due to crystallization of bio-organic phases on AgNPs surface. Even it was assumed that these extra peaks were probably due to metalloproteins, which act as strong X-ray diffraction centers [52, 53].

The antibacterial activity of *Streptomyces* sp. NS-33-synthesized AgNPs showed a good zone of inhibition against *S. aureus* and *S. pneumoniae*. This is because the AgNPs have a large surface area to volume ratio, which leads to better contact with microorganisms. Some researchers reported that due to the small size; the nanoparticles get attached and easily penetrate the bacterial cell wall. Furthermore, it was proved that cell membranes of microorganisms are composed of amino acids, phosphates, and carboxyl groups and hence provide a negative charge. This negative charge attracts slightly positively charged AgNPs and thereby causes the attachment to a bacterial cell wall. Inside the cell wall, the AgNPs impair the permeability of the plasma membrane and cause depletion of intracellular ATP by rupturing or by blocking respiration cycles. The AgNPs, after passing through the plasma membrane interact with sulfur-containing membrane proteins, phosphorous-containing compounds like DNA, and lipids. As a result of this, the cellular nucleic acids and proteins start dysfunctioning and finally lead to cell death. It was also noted that the AgNPs inhibit bacterial protein synthesis by attacking ribosomes and finally lead to their denaturation. Even the AgNPs are capable of producing large numbers of free radicals and reactive oxygen species (ROS), such as hydroxyl radicals, superoxide anions, hydrogen peroxide, singlet oxygen, and hypochlorous acid, attack the respiratory chains, and stop the production of antioxidant enzymes. Thus, the ROS and free radicals start accumulating in the bacterial cell and this accumulation finally leads to DNA damage and death of the bacterial cell [54, 55].

The toxic effects of *Streptomyces* sp. NS-33 synthesized AgNPs was determined based on their impact on the root meristematic cells of *A. cepa*. The review of the literature revealed that there was no report of cytotoxicity of AgNPs synthesized from actinomycetes. The meristematic cells showed different chromosomal aberrations during cell division at different concentrations of AgNPs (25 μg/ml, 50 μg/ml, 75 μg/ml, and 100 μg/ml). The result showed that as the MI was decreasing and chromosomal aberrations were increasing, the concentration of AgNPs was increasing from 25 to 100 μg/ml. This indicated the chromosomal abnormalities were directly proportional to the concentration of AgNPs. A similar concentration-dependent decrease in MI was also reported for TiO_2 nanoparticle-treated *A. cepa* root tip cells, which at a later stage led to DNA damage and induced oxidative stress. The reports on the toxicity of AgNPs can go as far as physiological implications, reproductive failure by modifying hormones, or hatching enzymes [56, 57]. It was also reported that the reduction in MI may be due to the blockage of the Gap-1 (G1) stage; that leads to the suppression of DNA synthesis. The presence of laggard chromosome was due to intervention of AgNPs in onion root tip cells, which might be having effect on spindle fibers and formation of acentric chromosomes. Due to the lack of a centromere and defected spindle fibers, the chromosomes start moving to opposite poles [58]. In the same way due to the presence of defected spindle fibers, the anaphasic sets of chromosomes do not lie in the same alignment [59]. The overall disturbances and depolymerisation of spindle fibers, shifting of poles, and change in the viscosity of cell cytoplasm may lead to disturbed metaphase, micronucleus formation, and chromosome break.

In some articles, the generation of ROS due to the accumulation of TiO_2 and Al_2O_3 nanoparticles within the cells was reported, which could thereby decrease the MI values [60]. AgNPs can enter into the environment through various ways, such as (a) release during the production of AgNPs and different nano-enabled products, (b) release during the use and after disposal of NP-containing products, and (c) through technical systems, such as wastewater treatment plants and landfills [61]. According to some researchers, these nanoparticles from soil translocate through xylem and accumulate through the food chain, which further transports in the plant cells through phloem or plasmodesmatal connections, ion channels, endocytosis, or aquaporins and impart toxicity to them [62, 63]. When the nanoparticles enter in

the cell through plasmodesmata, it changes the viscosity of cytoplasm, which leads to mitochondrial dysfunction and oxidative stress. Later, the nanoparticles power over the transportation of nutrients and other ions, which induce the toxicity to the cells. Thus, the nanoparticles pave the way for generation of ROS by altering the physiological characteristics within a cell and finally lead to cell death [62, 64].

5 Conclusions

The AgNPs were synthesized from soil *Streptomyces* sp. NS-33 and its genotoxicity on *A. cepa* was analyzed. A green synthesis method was employed for the synthesis of AgNPs. The green synthesis is an easy method and non-toxic to the environment when compared to the expensive and harmful chemical and physical methods. The molecular characterization of the strain confirmed its evolutionary relationship with *Streptomyces luteosporeus*. The characterizations of AgNPs using AFM, TEM, and XRD analysis revealed the size in the range of 22 to 78 nm. Moreover, FTIR spectra showed different functional groups, such as alkenes, alcohol, amine, esters carboxylic acid, alkane, and alkyl halide groups, which may be involved in capping, reducing, and stabilizing AgNPs. Later, the biosynthesized AgNPs displayed good antibacterial activity against two human pathogenic bacteria, such as *S. aureus* and *S. pneumoniae*. Therefore, this antibacterial efficacy of AgNPs can probably be utilized further for the production of antibacterial drugs or can also be used to eliminate the bacterial colonization on food transporting containers to protect and transport food safely without any contamination. The AgNP-treated *A. cepa* root tip cells indicated an AgNP dose-dependent decrease in MI and a gradual increase in chromosomal aberrations due to toxic effect. It is noted that the synthesized AgNPs have many adverse effects on various microorganisms as well as plants. Therefore, it is necessary to protect the entry of AgNPs in the ecosystem through proper maintenance and disposal of nanoparticles containing products. In future work a more systematic approach is required to unveil the adverse effects of AgNPs to the soil and ultimately to the ground water. Even a special attention is needed to perceive properly the impact of nanoparticles on ecosystems, functioning of ecosystems, communities, and ecosystem interactions across boundaries.

Abbreviations

AgNPs: Silver nanoparticles; *A. cepa*: *Allium cepa*; UV-Vis.: UV-visible; EDS: Energy dispersive spectroscopy; FTIR: Fourier transform infrared; G: Guanine; C: Cytosine; DNA: Deoxyribonucleic acid; IPCS: International Programme on Chemical Safety; WHO: World Health Organization; UNEP: United Nations Environment Programme; Ag: Silver; NaCl: Sodium chloride; SCA: Starch casein agar; ISP: International Streptomyces Project; SEM: Scanning electron microscope; H_2S: Hydrogen sulfide; 16S rRNA: 16S ribosomal ribonucleic acid; PCR: Polymerase chain reaction; dntps: Deoxyribonucleotide triphosphates; BLAST: Basic Local Alignment Search Tool; NCBI: National Center for Biotechnology Information; $AgNO_3$: Silver nitrate; AFM: Atomic force microscopy; TEM: Transmission electron microscope; XRD: X-ray diffraction; JCPDS: Joint Committee on Powder Diffraction Standards; MI: Mitotic index; SPSS-20: Statistical Package for the Social Sciences-20; ANOVA: Analysis of variance; SD: Standard deviation; SPR: Surface plasmon resonance

Acknowledgements

The authors of this article are grateful to the P.G. Dept. of Studies in Botany, Karnatak University, Dharwad, for extending laboratory facilities, and the authors are also acknowledged to University Scientific and Instrumentation Centre (USIC), Karnatak University, Dharwad, for providing necessary instruments facilities.

Authors' contributions

SN designed the research work and obtained the funding. BC, MPB, and BK performed the characterization of *Streptomyces* sp. NS-33. PSS, DA, and SKN performed the synthesis and characterization of AgNPs. BC wrote the manuscript. HH, MR, and DSB helped in interpretation of results. All the authors read and approved the manuscript.

Funding

None.

Availability of data and materials

The 16S rRNA gene sequence was submitted to NCBI (accession no. MN587998). The rest of the data can be provided by the authors upon reasonable request.

Ethics approval and consent to participate

Not applicable

Consent for publication

Not applicable

Competing interests

The authors of this article declare that they do not have any competing interests.

Received: 23 December 2019 Accepted: 1 September 2020
Published online: 24 November 2020

References

1. Feng XZ, Guo ZL, Wei S, Sangiliyandi G (2016) Silver nanoparticles: synthesis, characterization, properties, applications, and therapeutic approaches. Int J Mol Sci 17:1534. https://doi.org/10.3390/ijms17091534
2. Sang HL, Bong HJ (2019) Silver nanoparticles: synthesis and application for nanomedicine. Int J Mol Sci 20:865. https://doi.org/10.3390/ijms20040865
3. Veera BN, Jahnavi A, Rama K, Manisha RD, Rajkiran B, Pratap RMP (2013) Green synthesis of plant mediated silver nanoparticles using *Withania somnifera* leaf extract and evaluation of their antimicrobial activity. Int J Adv Res 1:307–313
4. Chen X, Schluesener HJ (2008) Nano-silver: a nanoproduct in medical application. Toxicol Lett 176:1–12. https://doi.org/10.1016/j.toxlet.2007.10.004
5. Rai M, Yadav A, Gade A (2009) Silver nanoparticles as a new generation of antimicrobials. Biotechnol Adv 27:76–83. https://doi.org/10.1016/j.biotechadv.2008.09.002
6. Sahayaraj K, Rajesh S (2011) Bionanoparticles: Synthesis and antimicrobial applications. In: Mendez-Vilas A (ed) Science against microbial pathogens: communicating current research and technological advances, 1st edn. Formatex Research Center, Spain
7. Khwaja SS, Azamal H, Rifaqat AKR (2018) A review on biosynthesis of silver nanoparticles and their biocidal properties. J Nanobiotechnol 16:14. https://doi.org/10.1186/s12951-018-0334-5
8. Javed I, Banzeer AA, Tariq M, Safia H, Akhtar M, Sobia K (2019) Green synthesis and characterizations of nickel oxide nanoparticles using leaf extract of *Rhamnus virgata* and their potential biological applications. Appl Organometal Chem 33:e4950. https://doi.org/10.1002/aoc.4950
9. Neelu C (2018) In: Maaz K (ed) Silver nanoparticles: synthesis, characterization and applications, silver nanoparticles - fabrication,

characterization and applications. IntechOpen. https://doi.org/10.5772/intechopen.75611
10. Rajeshkumar S, Malarkodi C, Paulkumar K, Vanaja M, Gnanajobitha G, Annadurai G (2013) Intracellular and extracellular biosynthesis of silver nanoparticles by using marine bacteria *Vibrio alginolyticus*. J Nanosci Nanotechnol 3:21–25
11. Singh P, Kim YJ, Zhang D, Yang DC (2016) Biological synthesis of nanoparticles from plants and microorganisms. Trends Biotechnol 34:588–599. https://doi.org/10.1016/j.tibtech.2016.02.006
12. Gokulakrishnan R, Ravikumar S, Raj JA (2012) In vitro antibacterial potential of metal oxide nanoparticles against antibiotic resistant bacteria pathogens. Asian Pac J Trop Disease 2:411–413. https://doi.org/10.1016/S2222-1808(12)60089-9
13. Nasrollahi KH, Paurshamsian MP (2011) Antifungal activity of silver nanoparticles on some of fungi. Int J Nano Dim 1:233–239
14. Reza GH, Akbar SA, Attar H, Rezayat SSM (2011) Biological and non-biological methods for silver nanoparticles synthesis. Chem Biochem Eng Q 25:317–326
15. Patrycja G, Magdalena W, Avinash PI, Indarchand G, Hanna D, Mahendra R (2014) Biogenic synthesis of metal nanoparticles from Actinomycetes: biomedical applications and cytotoxicity. Appl Microbiol Biotechnol 98: 8083–8097. https://doi.org/10.1007/s00253-014-5953-7
16. Rajagopal G, Palaniappan S, Kannan S (2018) Marine actinobacteria: a concise account for young researchers. Indian J Geo-Mar Sci 47:541–547
17. Swati S, Abhay BF, Asha C (2019) Bioprospection of marine Actinomycetes: recent advances, challenges and future perspectives. Acta Oceanologica Sinica 38:1–17. https://doi.org/10.1007/s13131-018-1340-z
18. Ouchari L, Boukeskasse A, Bouizgarne B, Ouhdouch Y (2019) Antimicrobial potential of Actinomycetes isolated from unexplored hot Merzouga desert and their taxonomic diversity. Biology Open 8:bio035410. https://doi.org/10.1242/bio.035410
19. Kekuda TRP, Shobha KS, Onkarappa R (2010) Studies on antioxidant and antihelmintic activity of two *Streptomyces* species isolated from Western Ghat soils of Agumbe, Karnataka. J Pharm Res 3:26–29
20. Ravikumar S, Inbaneson SJ, Uthiraselvam M, Priya SR, Ramu A, Banerjee MB (2011) Diversity of endophytic Actinomycetes from Karangkadu mangrove ecosystem and its antibacterial potential against bacterial pathogens. J Pharm Res 4:294–296
21. Ahmad A, Mukherjee P, Senapati S, Mandal D, Khan MI, Kumar R, Sastry M (2003a) Extracellular biosynthesis of silver nanoparticles using the fungus *Fusarium oxysporum*. Colloids Surf B Biointerfaces 28:313–318. https://doi.org/10.1016/S0927-7765(02)00174-1
22. Hulkoti NI, Taranath TC (2014) Biosynthesis of nanoparticles using microbes-a review. Colloids Surf B Biointerfaces 121:474–483. https://doi.org/10.1016/j.colsurfb.2014.05.027
23. Zhang X, Yan S, Tyagi RD, Surampalli RY (2011) Synthesis of nanoparticles by microorganisms and their application in enhancing microbiological reaction rates. Chemosphere 82:489–494. https://doi.org/10.1016/j.chemosphere.2010.10.023
24. Taofeek AY, Musibau AA, Akeem A, Agbaje L, Tesleem BA, Iyabo CO, Samuel OO, Adewumi AA (2017) Safety evaluation of green synthesized *Cola nitida* pod, seed and seed shell extracts mediated silver nanoparticles (AgNPs) using *Allium cepa* assay. J Taibah Univ Sci 11:895–909. https://doi.org/10.1016/j.jtusci.2017.06.005
25. Taofeek AY, Musibau AA, Agbaje L, Tesleem BA, Iyabo CO, Jelili AB, Suliyat AA, Adewumi AA (2017) Cytogenotoxicity potentials of cocoa pod and bean mediated green synthesized silver nanoparticles on *Allium cepa* cells, Caryologia. Int J Cytol Cytosyst Cytogenet 70:366–377. https://doi.org/10.1080/00087114.2017.1370260
26. Rajeshwari A, Suresh S, Natarajan C, Amitava M (2016) Toxicity evaluation of gold nanoparticles using an *Allium cepa* bioassay. RSC Adv 6:24000–24009. https://doi.org/10.1039/C6RA04712B.
27. Liman R, Gokce UG, Akyil D, Eren Y, Konuk M (2012) Evaluation of genotoxic and mutagenic effects of aqueous extract from aerial parts of *Linaria genistifolia* sub sp. *genistifolia*. Rev Bras Farmacogn 22:541–548. https://doi.org/10.1590/S0102-695X2012005000028
28. Azharuddin D, Tarikere CT (2018) Characterization and cytotoxic effect of biogenic silver nanoparticles on mitotic chromosomes of *Drimia polyantha* (Blatt. & McCann) Stearn. Toxicol Rep 5:910–918. https://doi.org/10.1016/j.toxrep.2018.08.018
29. Liman R, Akyil D, Eren Y, Konuk M (2010) Testing of the mutagenicity and genotoxicity of metolcarb by using both Ames/*Salmonella* and *Allium* test. Chemosphere 80:1056–1061. https://doi.org/10.1016/j.chemosphere.2010.05.011
30. Ranjita D, Wahengbam R, Rictika D, Hridip KS, Debajit T (2018) Antimicrobial potentiality of actinobacteria isolated from two microbiologically unexplored forest ecosystems of Northeast India. BMC Microbiol 18:71. https://doi.org/10.1186/s12866-018-1215-7
31. Sarvanakumar P, John PPR, Veeramuthu D, Savarimuthu I (2012) Antibacterial activity of some Actinomycetes from Tamil Nadu, India. Asian Pac J Trop Biomed 2:936–943. https://doi.org/10.1016/S2221-1691(13)60003-9
32. Sohan S, Arnab P, Abhrajyoti G, Maitree B (2015) Antimicrobial activities of Actinomycetes isolated from unexplored regions of Sundarbans mangrove ecosystem. BMC Microbiol 15:170. https://doi.org/10.1186/s12866-015-0495-4
33. Priyanka S, Mohan CK, Debajit T (2016) Broad spectrum antimicrobial activity of forest-derived soil actinomycete, *Nocardia* sp. PB-52. Front Microbiol 7: 347. https://doi.org/10.3389/fmicb.2016.00347
34. Marzan LW, Mehjabeen H, Sohana AM, Yasmin A, Masudul ACAM (2017) Isolation and biochemical characterization of heavy-metal resistant bacteria from tannery effluent in Chittagong city, Bangladesh: Bioremediation viewpoint. Egypt J Aquat Res 43:65–74. https://doi.org/10.1016/j.ejar.2016.11.002
35. Sukanya MK, Saju KA, Praseetha PK, Sakthivel G (2013) Therapeutic potential of biologically reduced silver nanoparticles from actinomycete cultures. J Nanosci 2013:ID940719. https://doi.org/10.1155/2013/940719.
36. Kumar S, Stecher G, Tamura K (2016) MEGA 7: Molecular evolutionary genetics analysis version 7.0 for bigger datasets. Mol Biol Evol 33:1870–1874. https://doi.org/10.1093/molbev/msw054
37. Abdullah ADN, Kareem MGA, Mariadhas VA (2018) Characterization of silver nanomaterials derived from marine *Streptomyces* sp. Al-Dhabi-87 and its in vitro application against multidrug resistant and extended-spectrum beta-lactamase clinical pathogens. Nanomaterials 8:279. https://doi.org/10.3390/nano8050279
38. Madakka M, Jayaraju N, Rajesh N (2018) Mycosynthesis of silver nanoparticles and their characterization. Methods X 5:20–29. https://doi.org/10.1016/j.mex.2017.12.003
39. Shkryl YN, Veremeichik GN, Kamenev DG, Gorpenchenko TY, Yugay YA, Mashtalyar DV, Nepomnyaschiy AV, Avramenko TV, Karabtsov AA, Ivanov VV, Bulgakov VP, Gnedenkov SV, Kulchin YN, Zhuravlev YN (2017) Green synthesis of silver nanoparticles using transgenic *Nicotiana tabacum* callus culture expressing silicatein gene from marine sponge *Latrunculia oparinae*. Artif Cells Nanomed Biotechnol 46:1646–1658. https://doi.org/10.1080/21691401.2017.1388248
40. Banala RR, Nagati VB, Karnati PR (2015) Green synthesis and characterization of *Carica papaya* leaf extract coated silver nanoparticles through X-ray diffraction, electron microscopy and evaluation of bactericidal properties. Saud J Biol Sci 22:637–644. https://doi.org/10.1016/j.sjbs.2015.01.007
41. Majeed S, Abdullah MSB, Nanda A, Ansari MT (2016) In vitro study of the antibacterial and anticancer activities of silver nanoparticles synthesized from *Penicillium brevicompactum* (MTCC-1999). J Taibah Univ Sci 10:614–620. https://doi.org/10.1016/j.jtusci.2016.02.010
42. Yvonne M, Evi S (2019) Actinomycetes: the antibiotics producers. Antibiotics 8:105. https://doi.org/10.3390/antibiotics8030105
43. Sreenivasa N, Bidhayak C, Pallavi SS, Meghashyama PB, Dattatraya A, Dhanyakumara SB, Muthuraj R, Halaswamy H, Shashiraj KN, Chaitra M (2019) Isolation, characterization, and functional groups analysis of *Pseudoxanthomonas indica* RSA-23 from rhizosphere soil. J Appl Pharm Sci 9:101–106. https://doi.org/10.7324/JAPS.2019.91113
44. Locci R (1989) Streptomycetes and related genera. In: Williams ST, Sharpe ME, Holt JG (eds) Bergey's manual of systematic bacteriology. Williams and Wilkins, Baltimore, pp 2451–2493
45. Cox MJ, Cookson WOCM, Moffatt MF (2013) Sequencing the human microbiome in health and disease. Hum Mol Genet 22:88–94. https://doi.org/10.1093/hmg/ddt398
46. Ahmad A, Senapati S, Khan MI, Kumar R, Ramani R, Srinivas V, Sastry M (2003b) Intracellular synthesis of gold nanoparticles by a novel alkalotolerant actinomycetes, *Rhodococcus* species. Nanotechnol 14:824. https://doi.org/10.1088/0957-4484/14/7/323
47. Saminathan K (2015) Biosynthesis of silver nanoparticles using soil actinomycetes *Streptomyces* sp. Int J Curr Microbiol Appl Sci 4:1073–1083
48. Karthik L, Kumar G, Vishnu Kirthi A, Rahuman AA, Rao VB (2014) *Streptomyces* sp. LK3 mediated synthesis of silver nanoparticles and its

biomedical application. Bioprocess Biosyst Eng 37:261–267. https://doi.org/10.1007/s00449-013-0994-3
49. Asma S, Hamid S, Mehwish I, Syed ZH, Afshan K, Roheena A, Saima S, Shagufta N, Faiza S, Ayesha A, Asma C (2019) Size-controlled production of silver nanoparticles by *Aspergillus fumigatus* BTCB10: likely antibacterial and cytotoxic effects. J Nanomater 2019:ID5168698. https://doi.org/10.1155/2019/5168698
50. Ragaa AH, Mervat HH, Rasha AA, Salwa SB (2019) Synthesis and biological characterization of silver nanoparticles derived from the cyanobacterium *Oscillatoria limnetica*. Sci Rep 9:13071. https://doi.org/10.1038/s41598-019-49444-y
51. Masum MMI, Siddiqa MM, Ali KA, Zhang Y, Abdallah Y, Ibrahim E, Qiu W, Yan C, Li B (2019) Biogenic synthesis of silver nanoparticles using *Phyllanthus emblica* fruit extract and its inhibitory action against the pathogen *Acidovorax oryzae* strain RS-2 of rice bacterial brown stripe. Front Microbiol 10:820. https://doi.org/10.3389/fmicb.2019.00820
52. Mehta BK, Meenal C, Shrivastava BD (2017) Green synthesis of silver nanoparticles and their characterization by XRD. J Phy Conf Series 836: 012050. https://doi.org/10.1088/1742-6596/836/1/012050
53. Mohammed RS, Mujeeb K, Mufsir K, Abdulrahman A-W, Hamad ZA, Mohammed RHS, Jilani PS, Anis A, Adeem M, Merajuddin K, Syed FA (2018) Plant-extract-assisted green synthesis of silver nanoparticles using *Origanum vulgare* L. extract and their microbicidal activities. Sustainability 10:913. https://doi.org/10.3390/su10040913
54. Sondi I, Salopek SB (2004) Silver nanoparticles as antimicrobial agent: a case study on *E. coli* as a model for Gram-negative bacteria. J Colloid Interface Sci 275:177–182. https://doi.org/10.1016/j.jcis.2004.02.012
55. Qing Y, Cheng L, Li R, Liu G, Zhang Y, Tang X, Wang J, Liu H, Qin Y (2018) Potential antibacterial mechanism of silver nanoparticles and the optimization of orthopedic implants by advanced modification technologies. Int J Nanomed 13:3311–3327. https://doi.org/10.2147/ijn.s165125
56. Panda KK, Achary VMM, Krishnaveni R, Padhi BK, Sarangi SN, Sahu SN, Brahma BP (2011) In vitro biosynthesis and genotoxicity bioassay of silver nanoparticles using plants. Toxicol inVitro 25:1097–1105. https://doi.org/10.1016/j.tiv.2011.03.008
57. Nair PMG, Park SY, Lee SW, Choi J (2011) Differential expression of ribosomal protein gene, gonadotrophin releasing hormone gene and Balbiani ring protein gene in silver nanoparticles exposed Chironomus riparius. Aquat Toxicol 101:31–37. https://doi.org/10.1016/j.aquatox.2010.08.013
58. Hilada N, Jasmin M, Azra M, Kemajl K (2013) Chromosomal and nuclear alterations in root tip cells of *Allium Cepa* L. induced by alprazolam. Med Arh 67:388–392. https://doi.org/10.5455/medarh.2013.67.388-392
59. Ghamery EAA, Kholy EMA, Yousser EMAA (2003) Evaluation of cytological effects of Zn2+ in relation to germination and root growth of *Nigella sativa* L. and *Triticum aestivum* L. 537:29–41. https://doi.org/10.1016/s1383-5718(03)00052-4
60. Rajeshwari A, Kavitha S, Alex SA, Kumar D, Mukherjee A, Chandrasekaran N, Mukherjee A (2015) Cytotoxicity of aluminum oxide nanoparticles on *Allium cepa* root tip-effects of oxidative stress generation and biouptake. Environ Sci Pollut Res 22:11057–11060. https://doi.org/10.1007/s11356-015-4355-4
61. Gottschalk F, Sonderer T, Scholz RW, Nowack B (2009) Modeled environmental concentrations of engineered nanomaterials (TiO_2, ZnO, Ag, CNT, Fullerenes) for different regions. Environ Sci Technol 43:9216–9222. https://doi.org/10.1021/es9015553
62. Tripathi DK, Singh S, Singh S, Srivastava PK, Singh VP, Singh S, Prasad SM, Singh PK, Dubey NK, Pandey AC, Chauhan DK (2017) Nitric oxide alleviates silver nanoparticles (AgNps)-induced phytotoxicity in *Pisum sativum* seedlings. Plant Physiol Biochem110:167-177. https://doi.org/10.1016/j.plaphy.2016.06.015.
63. Guangshu Z, Katherine SW, David WP, Pedro JJA, Jerald LS (2014) Transport of gold nanoparticles through plasmodesmata and precipitation of gold ions in woody poplar. Environ Sci Technol Lett 1:146–151. https://doi.org/10.1021/ez400202b
64. Attwood ST, Unrine JM, Stone JW, Murphy CJ, Ghoshroy S, Blom D, Bertsch PM, Newman LA (2012) Uptake, distribution and toxicity of gold nanoparticles in tobacco (*Nicotiana xanthi*) seedlings. Nanotoxicol 6:353–360. https://doi.org/10.3109/17435390.2011.579631

Publisher's Note